applied sciences

MDPI

Article

Modeling and Simulation of a Hybrid Compression/Absorption Chiller Driven by Stirling Engine and Solar Dish Collector

Guerlin Romage [1], Cuauhtémoc Jiménez [2,3], José de Jesús Reyes [2,3], Alejandro Zacarías [3,*], Ignacio Carvajal [2], José Alfredo Jiménez [2], Jorge Pineda [4] and María Venegas [5]

1 Instituto Politécnico Nacional, Centro Mexicano para la Producción más Limpia CMP+L, Av. Acueducto S/N, Ticomán, Mexico City 07340, Mexico; guerlin@hotmail.com
2 Instituto Politécnico Nacional, ESIME UPALM, Mexico City 07738, Mexico; cjimenezc@ipn.mx (C.J.); jerz70@gmail.com (J.d.J.R.); icarvajal@ipn.mx (I.C.); jjimenezb@ipn.mx (J.A.J.)
3 ESIME Azcapotzalco, Instituto Politécnico Nacional, Av. de las Granjas 682, Santa Catarina, Mexico City 02250, Mexico
4 CICATA Querétaro, Instituto Politécnico Nacional, Cerro Blanco 141, Colinas del Cimatario, Querétaro 76090, Mexico; jpinedap@ipn.mx
5 Departamento de Ingeniería Térmica y de Fluidos, Universidad Carlos III de Madrid, Avda. Universidad 30, Leganés, 28911 Madrid, Spain; mvenegas@ing.uc3m.es
* Correspondence: azacarias@ipn.mx; Tel.: +52-5544-884-217

Received: 19 November 2020; Accepted: 15 December 2020; Published: 17 December 2020

Featured Application: Absorption and compression cooling systems fed by solar thermal energy.

Abstract: In this paper, an evaluation of the performance and operating parameters of a hybrid compression/absorption chiller coupled with a low-capacity solar concentrator is presented. The study was carried out using energy and mass balances applied to each component of each system. The variables evaluated in the hybrid chiller were the cooling power, the supply power, the Coefficient of Performance (COP) of both cooling systems and the ratio between heat and power. The diameter and temperature of the hot spot as well as the performance of the dish collector were evaluated. The changed parameters were the heat removed by each refrigeration system, the condenser temperature, the evaporator temperature, the concentration ratio and the irradiance. Results have shown that the compression system can produce up to 53% more cooling power than the heat supplied to the hybrid system. Meanwhile, the absorption system produces approximately 20% less cooling power than the supplied heat. It has also been found that, for the cooling power produced by the hybrid cooler to be always greater than the heat supplied, the cooling power provided by the absorption system should preferably be between 20% and 60% of the total, with a Stirling engine efficiency between 0.2 and 0.3 and a condensation temperature from 28 to 37 °C. Likewise, it has been found that the compression system can produce cooling power up to 3 times higher than the heat of the Stirling engine hot source, with T_h = 200 °C and η_s = 0.3. Finally, it has been found that, in a low-capacity solar concentrator, on a typical day in Mexico City, temperatures in the hot spot between 200 and 400 °C can be reached with measured irradiance values from 200 to 1200 W/m^2.

Keywords: hybrid chiller; compression/absorption chiller; stirling engine; solar collector

1. Introduction

Constantly, efforts to reduce energy consumption in residential and commercial buildings are mainly due to the fact that such buildings consume up to 40% of the available energy, as shown by [1]. Likewise, authors of [2] ensure that residential, commercial, public and service buildings consume up to 54% of available energy. Various studies have been carried out to reduce energy consumption in residential buildings, and an example can be seen in the work published by [3]. The work present by [1] has shown that, using tubes embedded in the wall, the costs and energy consumption can be reduced. The system was controlled by a specialized program that synchronizes the supply and extraction heat. On the other hand, the author of [4] has shown that, for heating and cooling systems, it is possible to achieve a high share of renewable energies using hybrid systems. Additionally, [5] evaluated a cogeneration and cooling system where heat was obtained through geothermal energy and solar energy, reaching a COP of 3.81. Likewise [6] investigated a technology in district cooling systems, in which it is possible to use renewable energies such as solar thermal energy. Works on hybrid cooling systems have been published by [7], in which the authors have shown that energy saving may exceed 60% when the latent load in the conditioned space is high. As has been shown so far, studies of hybrid compression/absorption cooling systems have already been carried out by different researchers, where electrical energy is used as supply energy.

On the other hand, the ability of Stirling engines to transform low-enthalpy solar energy into mechanical energy makes them ideal for application in low-capacity installations. The Stirling engine has been used in compression refrigeration systems for domestic use due to its low noise level and wide range of use of renewable energy sources such as solar energy, as shown by [8–10]. In the same way, parabolic disk collectors are used with Stirling engines and domestic air conditioning systems, due to their capacity and small size, as shown by [11,12]. As can be seen in [13,14], Stirling engine cooling can be produced using solar energy.

Absorption refrigeration systems coupled with another refrigeration system have been published by [15–18]. Solar absorption cooling systems play an important role in energy saving and emission reduction in buildings, as [19] showed. The authors showed that this equipment has better energy saving performance and less environmental impact. [20] proposed a novel solar absorption-compression cascade refrigeration system. The researchers found that energy consumption decreases by 26.7%. The modeling and simulation of hybrid solar absorption/compression cooling systems has been carried out by researchers such as [21,22]. The authors have shown that the cooling power is strongly dependent on the compressor speed. Whereas, at high temperature and low flow rate of the cooling water in the compression system, the performance of the hybrid system is adverse. Absorption cooling systems powered by solar concentrators are increasingly being studied. Results published by [23] show that traditional single-effect and double-effect absorption chillers have a relatively small operating temperature range, which limits the application of solar systems. For this reason, they propose a novel solar system that integrates photovoltaic and photothermic solar collectors.

As far as it has been possible to know, in all the works shown here, flat plate solar collectors or channel concentrators have been used for the power supply and generally for cooling capacities greater than 20 kW. In the present work, a hybrid compression/absorption chiller driven by a Stirling engine and a dish solar collector has been thermodynamically evaluated. A dish solar collector has been chosen over a parabolic trough one, mainly because in the former the Stirling engine can be better coupled to the circular focus. Likewise, a dish solar collector provides heat at a higher temperature than a flat solar collector and takes better advantage of a solar track compared to a channel one. On the other hand, traditional air conditioning equipment requires electrical energy in the compressor motor for its operation, which increases the daily consumption of electricity and the cost of operation. The hybrid cooler proposed here consumes a negligible amount of electrical energy in the solution pump, due to the fact that the compressor is driven by the Stirling engine and it is powered by solar thermal energy.

The study has been carried out for two cases. In the first case (Sections 2.1 and 3.1), the thermal energy required by the absorption system and the Stirling engine has been determined as a function of

the cooling capacity of the conditioned space, the outside temperature and the generation temperature. In the second case (Sections 2.2 and 3.2), solar radiation and collector temperature were measured, and the cooling power produced by a compression/absorption system fed by a low-capacity solar concentrator was evaluated, depending on the solar radiation and the concentration ratio.

2. Modeling and Simulation

The hybrid compression/absorption chiller and the low-capacity solar concentrator analyzed in this work are shown in Figure 1. The chiller is made up of the following 5 systems:

- Space conditioning system, SCS. In this system, it is required to remove the heat from the conditioned Space conditioning system, SCS. In this system, it is required to remove the heat from the conditioned space. Solar radiation and outside temperature influence the amount of heat to be removed by the coil $\dot{Q}_e$.
- Compression refrigeration system, CRS. This system removes the heat from the conditioned space through the evaporator $\dot{Q}_{ce}$. This parameter, together with the outside temperature, T_o, and the inside temperature, T_i, influences the power of the compressor, $\dot{W}_c$.
- Thermal engine system, TES. This system consists of a Stirling engine mechanically coupled to the compressor of the compression system. Depending on the power of the compressor and the efficiency of the heat engine, the amount of heat required from the hot source $\dot{Q}_{HS}$ is determined.
- Absorption refrigeration system, ARS. This system removes the heat from the conditioned space through $\dot{Q}_{ae}$. This parameter, together with the outside temperature, inside temperature and supply temperature, T_g, influences the amount of heat required in the generator $\dot{Q}_g$.
- Solar energy system, SES. This system consists of a dish collector, which takes advantage of the radiation in the heat absorber. This heat is provided to the Stirling engine that is coupled to the compression system and/or the absorption refrigeration system.

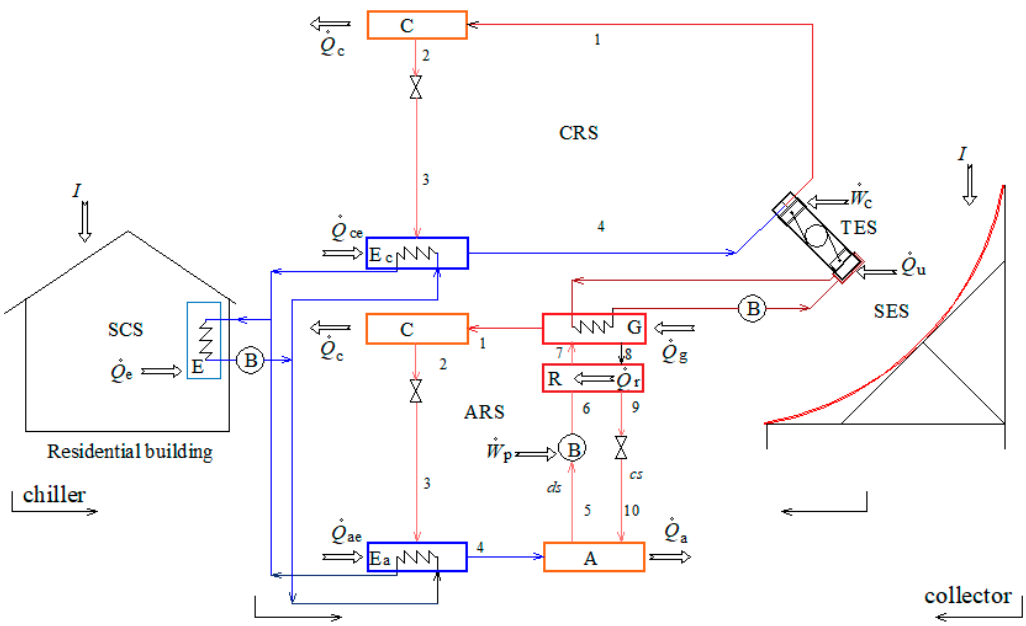

Figure 1. Schematic diagram of the hybrid compression/absorption chiller fed by Stirling engine and solar energy.

Modeling of each component and each system is shown in Section 2.1. Modeling of the dish collector is shown in Section 2.2.

2.1. Modeling of Hybrid Compression/Absorption Chiller

2.1.1. Space Conditioning System, SCS

The model of the conditioned space was made as shown below. The amount of heat to remove in a conditioned space, $\dot{Q}_T$, is given by

$$\dot{Q}_T = \dot{Q}_t + \dot{Q}_r + \dot{Q}_{inf} + \dot{Q}_{oc} + \dot{Q}_{misc} \tag{1}$$

where, $\dot{Q}_t$ is determined as shown by [24], in the form

$$\dot{Q}_t = UA(T_o - T_i) \tag{2}$$

$$\dot{Q}_r = A_{sup}\varepsilon\sigma\left(T_s^4 - T_o^4\right) \tag{3}$$

T_s, T_o and T_i are the temperature on the surface, outside and inside of the conditioned space, respectively. U and A are, respectively, the global heat transfer coefficient and the area of walls and ceiling. A_{sup}, is the area exposed to solar radiation. ε and σ are, respectively, the emissivity coefficient and the Stefan Boltzman's constant. $\dot{Q}_{inf}$ is the infiltration load, $\dot{Q}_{oc}$, is the load due to occupants, and $\dot{Q}_{misc}$ is the load due to miscellaneous.

Heat from the conditioned space is removed by both the absorption system and the compression system:

$$\dot{Q}_e = \dot{Q}_{ae} + \dot{Q}_{ce} \tag{4}$$

The fraction of heat, x, that each refrigeration system can remove, is represented by

$$x_a = \frac{\dot{Q}_{ae}}{\dot{Q}_e};\ x_c = \frac{\dot{Q}_{ce}}{\dot{Q}_e} \tag{5}$$

Therefore, the total heat removed is

$$\dot{Q}_T = x_a\dot{Q}_e + x_c\dot{Q}_e \tag{6}$$

$$\text{where } x_c = (1 - x_a) \tag{7}$$

2.1.2. Compression Refrigeration System, CRS

From Equations (5)–(7), the heat removed by the compression system $\dot{Q}_{ce}$ is determined.

Refrigerant flow in this system, $\dot{m}_{cr}$, is determined by

$$\dot{Q}_{ce} = \dot{m}_{cr}(h_4 - h_3) \tag{8}$$

where h_3 and h_4 are the enthalpies in the evaporator.

Compressor power is computed from

$$\dot{W}_c = \dot{m}_{cr}(h_1 - h_4) \tag{9}$$

Entalpies h_1 and h_4 are those of the refrigerant at the compressor outlet and inlet, respectively.

Coefficient of performance was computed from

$$COP_c = \frac{\dot{Q}_{ce}}{\dot{W}_c} \tag{10}$$

2.1.3. Thermal Engine System, TES

Power required by the compression system is provided by the heat engine, as Stirling engine power, $\dot{W}_S$. Heat of the Stirling engine hot source, $\dot{Q}_{HS}$, is determined from the performance equation shown by [14]

$$\eta_s = \frac{\dot{W}_s}{\dot{Q}_{HS}} \tag{11}$$

In the present work, the performance of the Stirling engine was varied between 0.1 and 0.3. These values were taken from the work published by [14].

Heat transferred to the cold sink, $\dot{Q}_{LS}$, is determined from

$$\dot{W}_s = \dot{Q}_{HS} + \dot{Q}_{LS} \tag{12}$$

2.1.4. Absorption Refrigeration System, ARS

From Equations (4)–(6) the heat to be removed by the evaporator of the absorption system, $\dot{Q}_{ae}$, is determined. Refrigerant flow of this refrigeration system is determined from

$$\dot{Q}_{ae} = \dot{m}_{ar}(h_4 - h_3) \tag{13}$$

where the enthalpies h_3 and h_4 are those of the refrigerant, at the inlet and outlet, respectively.

Mass flow rate of the diluted solution is determined as shown by [25–27], as

$$\dot{m}_{ds} = \dot{m}_{ar}\frac{X_{cs}}{X_{cs} - X_{ds}} \tag{14}$$

Pump power is determined, as shown by [26], by

$$\dot{W}_p = \frac{(P_6 - P_5)v_{ds}\,\dot{m}_{ds}}{\eta_m} \tag{15}$$

Specific work of the pump is related to enthalpy and power by

$$w = (h_6 - h_5); w = \frac{\dot{W}_p}{\dot{m}_{ds}} \tag{16}$$

In the recuperator, the heat flow is

$$\dot{Q}_{re} = \dot{m}_{ds}(h_7 - h_6) \tag{17}$$

$$\dot{Q}_{re} = \dot{m}_{cs}(h_8 - h_9) \tag{18}$$

$$\varepsilon_{re} = \frac{T_7 - T_6}{T_8 - T_6} \tag{19}$$

The following relationships are valid in the generator and absorber, respectively.

$$\dot{m}_{ds}\,X_7 = \dot{m}_{cs}\,X_8 + \dot{m}_{ar}\,X_1 \tag{20}$$

$$\dot{m}_{ds} = \dot{m}_{cs} + \dot{m}_{ar};\ \dot{m}_{ds}\,X_5 = \dot{m}_{cs}\,X_{10} + \dot{m}_{ar}\,X_4 \tag{21}$$

Heat flux in each component is

$$\dot{Q}_c = \dot{m}_{ar}(h_1 - h_2) \tag{22}$$

$$\dot{Q}_a = \dot{m}_{ar}\,h_4 + \dot{m}_{cs}\,h_{10} - \dot{m}_{ds}\,h_5 \tag{23}$$

$$\dot{Q}_g = \dot{m}_{ar}\, h_1 + \dot{m}_{cs}\, h_8 - \dot{m}_{ds}\, h_7 \tag{24}$$

Coefficient of performance is

$$COP_a = \frac{\dot{Q}_{ae}}{\dot{Q}_g + \dot{W}_p} \tag{25}$$

The supply heat for the hybrid cooler, $\dot{Q}_D$, is the sum of the heat required by the hot source of the Stirling engine, $\dot{Q}_{HS}$, and the heat required by the generator, $\dot{Q}_g$, of the absorption system, as

$$\dot{Q}_D = \dot{Q}_{HS} + \dot{Q}_g \tag{26}$$

2.2. Modeling of the Solar Collector for Hybrid Chiller

Solar Energy System, SES

Modeling of the solar collector was carried out as follows. In the solar energy system, the concentration ratio, C, is the ratio between the area of the parabolic disk, A_{app}, and the area of the solar absorber (or hot spot), A_{ab}, as

$$C = \frac{A_{app}}{A_{ab}} \tag{27}$$

Useful heat of the solar concentrator can be determined, as shown by [28], by Equation (28).

$$\dot{Q}_u = IA_{app}\eta_o - A_{ab}\left[h(T_h - T_o) + \varepsilon\sigma\left(T_h^4 - T_o^4\right)\right] \tag{28}$$

where I is the irradiance, η_o is the optical efficiency of the concentrator. h, ε and σ are, respectively, the radiation heat transfer coefficient, the emissivity of the hot spot and the Stefan Boltzmann's constant. T_h and T_o are the temperatures of the hot spot of the solar concentrator and of the ambient air, respectively.

Solar collector performance is determined by the equation

$$\eta_s = \frac{\dot{Q}_u}{IA_{app}} = \eta_o - \frac{1}{IC}\left[h(T_h - T_o) + \varepsilon\sigma\left(T_h^4 - T_o^4\right)\right] \tag{29}$$

After determining the useful heat of the solar collector, the heat fed to the hot source of the Stirling engine is determined using Equations (26) and (30). In this last equation, x_g and x_{St} indicate the fraction of useful heat used by the absorption system and by the Stirling engine, respectively.

$$x_g = \frac{\dot{Q}_g}{\dot{Q}_u};\ x_{St} = \frac{\dot{Q}_S}{\dot{Q}_u} \tag{30}$$

Using Equations (13)–(24), the mass flow rates of diluted solution, concentrated solution, refrigerant, as well as the thermodynamic properties and temperatures of the fluids are determined. With these, the cooling power produced by the absorption system, $\dot{Q}_{ae}$, can be determined.

Using Equations (11) and (12) and the heat of the hot source, $\dot{Q}_{HS}$, the power of the compressor in the compression refrigeration system, $\dot{W}_c$, is determined. Using Equations (8) and (9) and the thermodynamic properties of the refrigerant, the cooling power that can be produced by the compression system coupled to the Stirling engine, $\dot{Q}_{ce}$, is determined.

2.3. Assumptions

Conditioned space assumptions. Temperature of the surface of the conditioned space, T_s, was considered $T_s = (T_o + T_i)/2$.

The constant parameter, $\dot{Q}_{const}$, includes $\dot{Q}_{inf}$, $\dot{Q}_{oc}$ and $\dot{Q}_{misc}$, which are considered not to vary with respect to solar radiation and outside temperature. Therefore, this parameter was written as

$$\dot{Q}_{const} = \dot{Q}_{inf} + \dot{Q}_{oc} + \dot{Q}_{misc} \tag{31}$$

Surfaces exposed to the sun were the roof and the south, east and west walls (a multiplying factor of 0.5 was added to the last two walls, because they are not exposed to the sun during all solar hours).

Compression system assumptions. The compression system is modeled by an ideal cycle. At the outlet of the condenser and evaporator the refrigerant is in saturated state. Isenthalpic process in the expansion valve and isentropic process in the compressor occur. Condensation temperature was considered as $T_c = T_o + 5$ °C.

Thermal engine system assumptions. Friction and heat losses in the mechanical coupling between the Stirling engine and the compressor of the compression system are negligible. The authors in [28] have shown that the maximum efficiency of the Stirling engine is 0.3. Likewise, [29] have ensured that in a Stirling engine, 36.24% of the energy is lost in the thermodynamic cycle, while 37.52% is thermally lost. Therefore, in this work, it is considered that $T_{HS} = T_h - 50$ °C and $T_g = T_{HS} - 50$ °C.

Absorption refrigeration system assumptions. The absorption system is modeled by an ideal cycle. Saturation conditions of working fluids exist at the outlet of generator, condenser, absorber and evaporator. Isenthalpic process in valves and isentropic process in the pump occur. Friction and thermal losses are negligible.

Solar energy system assumptions. The optic efficiency is $\eta_o = 0.90$, taken from [28].

2.4. Hybrid Chiller Simulation

Models developed in Sections 2.1 and 2.2 have been programmed in the specialized software Engineering Equation Solver, EES, [30].

Refrigerants used in the compression and absorption systems were, respectively, R134a and R718. Solution used in the absorption system was water-lithium bromide. Properties of the refrigerants and the solution were determined using the EES software. Specifications of the conditioned space and the solar concentrator are shown in Table 1.

Table 1. Conditioned space and solar collector specifications.

Parameter	Value
Conditioned space	
Dimensions: length, wide, heigh [m]	4, 3, 2.5
Global heat transfer coefficient, U, [W/m^2 K]	0.5
Solar collector	
Focus height, h [m]	0.88
Dish diameter, D [m]. Data taken from [31]	1.4
Optical efficiency, η_o, [ ]. Data taken from [28]	0.85
Emissivity of the dish, ε	0.9

For the simulation of the hybrid cooler and the solar concentrator, the parameters shown in Table 2 were varied according to the values presented.

Table 2. Parameters changed for the simulation.

Parameter	Value
Evaporation temperature, T_e, °C	5, 10, 15
Condensation temperature, T_c, °C	28, 32, 37
Irradiance, I, W/m^2	200–1000
Concentration ratio, C	5–100
Operating fraction of the absorption system, x_a	0.01–0.99

2.5. Model Validation

The model developed in this section is based on fundamental equations of thermodynamics, heat transfer and refrigeration cycles. Therefore, the model can be valid in all simulated conditions, allowing a qualitative analysis of the system performance under different conditions. A full system validation is not possible because the proposed systems is new and there are no experimental facilities of this type available. However, as far as it is possible, this section shows the analysis of COP of compression and absorption refrigeration systems, with x_a = 0.31, η_s = 0.3 and T_g = 90 °C, at different conditions of T_c and T_e. The absorption system COP is compared with the results of a single effect absorption refrigeration system, published by [27]. It can be seen in Figure 2 that, with T_e = 5 °C and T_g = 90 °C, the COP has values very close to those published by the authors.

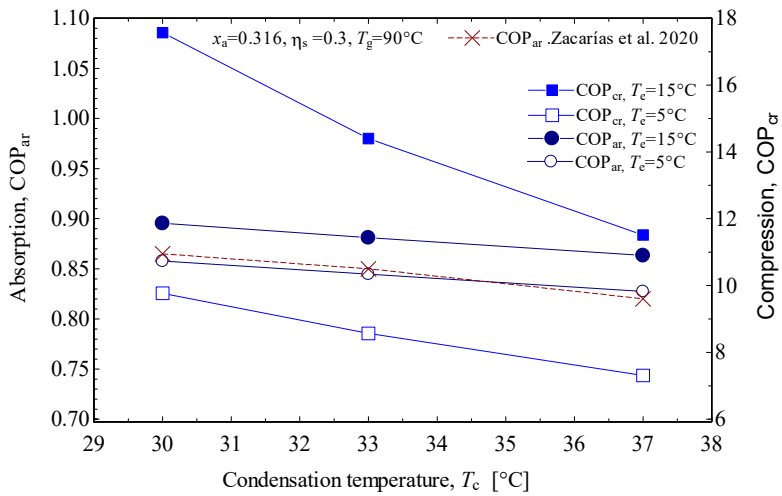

Figure 2. Hybrid chiller coefficient of performance (COP) and COP$_{ar}$ validation as a function of T_c.

3. Results

The results obtained from the modeling and simulation of the hybrid chiller are shown in Figures 3–5, while those corresponding to the solar collector simulation are shown in Section 3.2. The study of the solar collector was supported by radiation and temperature data measured in a solar concentrator in Mexico City.

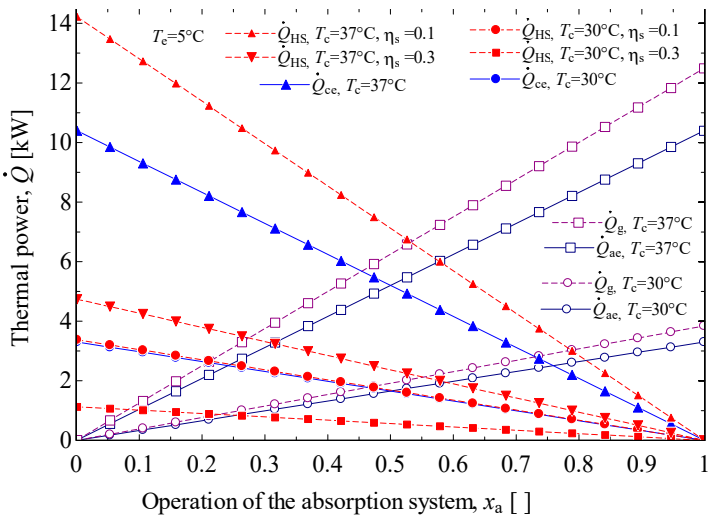

Figure 3. Cooling and supply heat in the hybrid chiller relative to the operating ratio of the cooling systems, x_a.

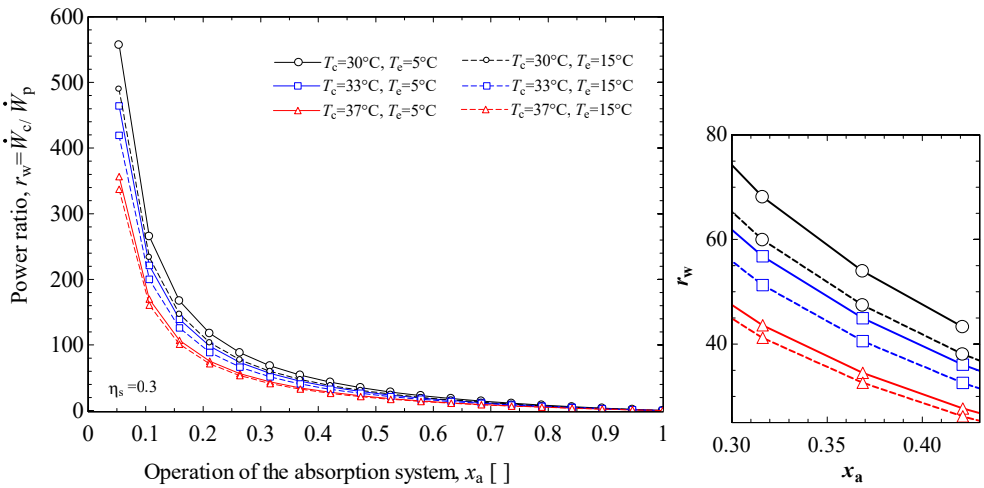

Figure 4. Power ratio of the compressor to solution pump with respect to the operating ratio of the refrigeration systems, x_a.

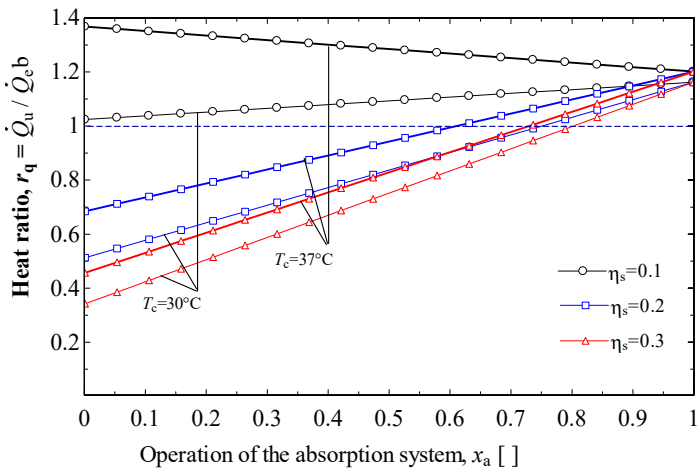

Figure 5. Useful heat to cooling power ratio versus absorption system operating ratio, x_a.

3.1. Hybrid Compression/Absorption Chiller

Figure 3 shows the results of the cooling supplied to the conditioned space by the absorption system, $\dot{Q}_{ae}$, and by the compression system coupled to the Stirling engine, $\dot{Q}_{ce}$, considering the operating range of the refrigeration systems, from $x_a = 0$ to $x_a = 1$. It also shows the heat required in the generator of the absorption system, $\dot{Q}_g$, and that required in the hot source of the Stirling engine, $\dot{Q}_{HS}$, that moves the compression refrigeration system. In the figure, it can be seen that the heat demanded by the two cooling systems is equal when $x_a = 0.5$. When the absorption system is not operated ($x_a = 0$), the compression system provides 100% of the cooling demand, while when the absorption system operates at 100% ($x_a = 1$), the compression system does not operate. The heat demanded by each refrigeration system for its operation changes in a different way. The heat demanded by the generator of the absorption system is greater than the cooling power produced by approximately 13% and 16% at 28 and 37 °C, respectively, of condensation temperature. On the other hand, the heat required by the Stirling engine to feed the compression refrigeration system is greater than the cooling power produced by approximately 2.9% and 27.9% at 28 and 37 °C, respectively, if the heat engine operates with an efficiency of 0.1. However, if this heat engine operates with an efficiency of 0.3, the heat required as input by the Stirling engine is less than the cooling power produced, up to 66.6 and 53.4% at 28 and 37 °C in the condenser, respectively. This means that, if the conditioned space is required to be cooled only by the absorption system, approximately 16% more heat is required in the supply to this system. Whereas, if the cooling occurs only with the compression system coupled to the Stirling engine, the heat required by the system may be less than the cooling produced (up to 53.8% if the engine operates with an efficiency of 0.3 and 37 °C at the condenser). This is due to the good performance of the compression system.

The power ratio of the compressor to the pump of the compression and absorption system, respectively, is shown in Figure 4, for the entire operating range of the chiller, from $x_a = 0$ to $x_a = 1$. When the absorption system operates at 5% ($x_a = 0.05$), the power ratio is approximately 560, with $T_c = 30$ °C and $T_e = 5$ °C. At the same temperature in the condenser and $T_e = 15$ °C, the power ratio is approximately 490. This is due to the minimal power required by the pump of the absorption system and because the cooling required in the conditioned space is supplied almost entirely by the compression system. This power ratio decreases from about 130 to 30 in the range from $x_a = 0.2$ to $x_a = 0.45$. The power ratio is reduced to approximately 5, when the absorption system operates at approximately 95%. According to this figure, it is recommended to operate the hybrid cooler from $x_a = 0.2$ to $x_a = 1$.

Figure 5 shows the relationship between the useful heat generated by the solar concentrator and the cooling power produced by the hybrid cooler throughout the entire operating range of the system, from $x_a = 0$ to $x_a = 1$. From the figure, it can be seen that if the efficiency of the Stirling engine is 0.1, the heat supplied to the global system is greater than the cooling power produced ($r_q > 1$). This means that more heat is supplied than cold is produced. Whereas, if the efficiency of the heat engine is 0.2 and 0.3, the heat supplied to the global system is less than the cooling power produced in the operating range from $x_a = 0$ to $x_a = 0.65$ and $x_a = 0.8$, respectively. After these values, in all cases of efficiency and condensation temperature analyzed in this work, the heat supplied to the hybrid system is greater than the cooling power produced. From Figure 5, it can be concluded that the operation of the hybrid cooler should be between $x_a = 0$ and $x_a = 0.80$ if the efficiency of the Stirling engine is 0.3. This conclusion is based on the objective of always producing greater cooling than heat supplied to the system ($\dot{Q}_e > \dot{Q}_u$ and $r_q < 1$).

From Figures 3–5, it can be concluded that it is convenient to operate the hybrid cooler in the operating range from $x_a = 0.2$ to $x_a = 0.4$, so that the power ratio is not much greater than 100 and the cooling power produced is always greater than the heat supplied. In the recommended range, the cooling output is approximately 50–70% greater than the heat supplied.

3.2. Solar Collector for Hybrid Chiller

Before performing the simulation of the solar collector, the hot temperature of the solar collector was measured. The values of radiation and temperatures measured for a typical day in Mexico City are shown in Figure 6. The measurements were made with a type K thermocouple and a direct radiation meter TM-206 MCA TENMARS. The accuracy of the thermocouple and pyrometer are, respectively, ±0.75% and ± 10 W/m^2 (or 5%, whichever is greater in sunlight). Measurements were made every 30 min. The value of each variable was saved when data were stable for at least 30 s. From the figure, it can be seen that the ambient temperature and radiation, respectively, were between 21 and 28 °C and 600 and 1200 W/m^2 during the day. With these radiation and ambient temperature values, it was possible to measure temperature values in the hot spot of approximately 200 to 400 °C. In the figure, the value of radiation at 14:00 is lower because the instrument used measures instantaneous radiation. In this case, the meter display was obstructed by a cloud. This was not an obstacle for the temperature at that time to remain at the maximum value of 400 °C approximately.

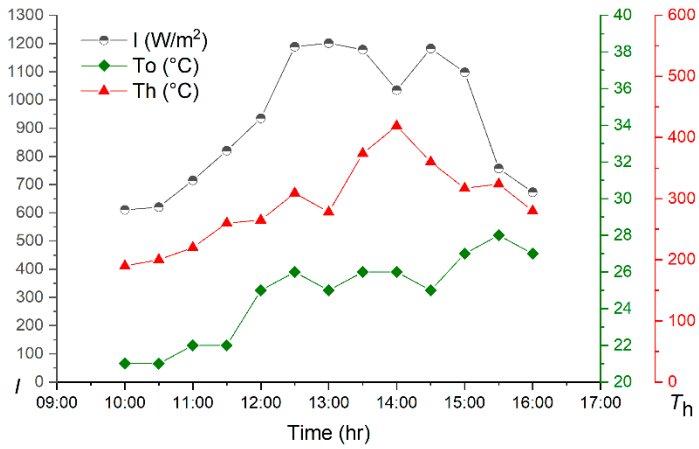

Figure 6. Radiation and temperature values measured in the solar concentrator during a typical day in Mexico City.

The results of the low-capacity solar concentrator modeled in Section 2.2 are shown in this section. Figure 7 shows the area and diameter of the solar absorber obtained as a function of the concentration ratio, C, varying from 5 to 100. It can be seen that the area and diameter of the absorber decrease at a rate of 2.5% and 1.66%, respectively, for each concentration unit between the values of C = 20 and C = 40. For higher values of the concentration ratio, the decrease ratio is 1.1% and 1.0% for the area and the diameter, respectively. For concentration ratios lower than 10, the area and the diameter decrease at a rate of 10.66% and 5.8%, respectively, for each unit of concentration ratio increment. These results suggest that, with concentration ratios greater than 20, the diameter of the absorber will be less than 30 cm. This can contribute to the radiation in the hot source being distributed over a larger area, reaching medium temperatures, rather than high temperatures, which contributes to improving the efficiency of the solar concentrator, as shown below.

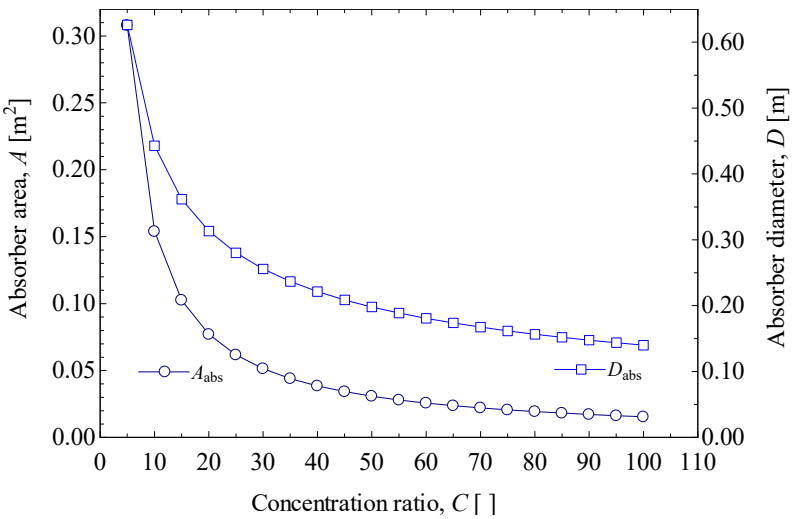

Figure 7. Area and diameter of the solar absorber in relation to the concentration ratio.

Heat supplied to the hybrid system and cooling power produced by both cooling systems are shown in Figure 8, for a temperature in the solar collector of 200 °C and 40% of the heat produced supplied to the absorption cooling system, x_g = 0.4. In the same figure, with I = 1000 W/m^2, it can be seen that the cooling produced by the absorption cooling system is approximately 11% less than the heat supplied to the generator. However, the compression system can produce 1, and up to 2 and 3 times more cooling than the heat supplied to the Stirling engine hot source, with efficiencies in this thermal engine of 0.1, 0.2 and 0.3, respectively.

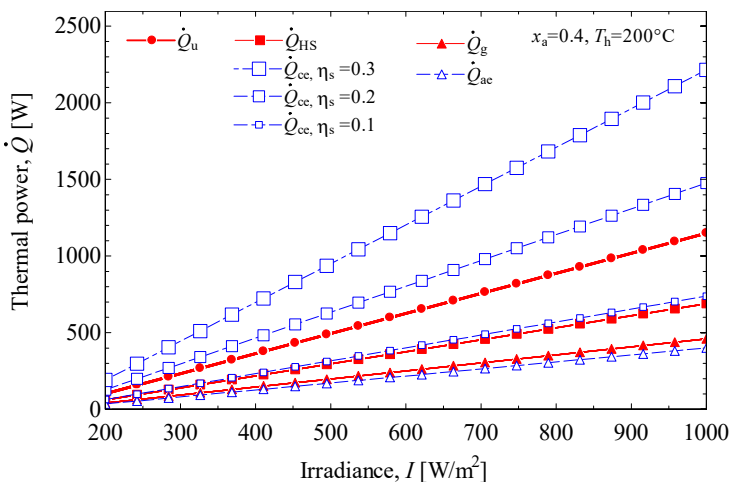

Figure 8. Thermal power produced by the solar concentrator and by absorption/compression refrigeration systems, with respect to solar radiation.

The efficiency of the solar concentrator, shown in Figure 9, was evaluated at temperatures in the hot spot, T_h, of 200, 300 and 400 °C. From the figure it can be seen that, in the radiation range from 200 to 1000 W/m^2 and C = 30, the efficiency decreases faster when the temperature of the hot spot is 400 °C than when it is 200 °C.

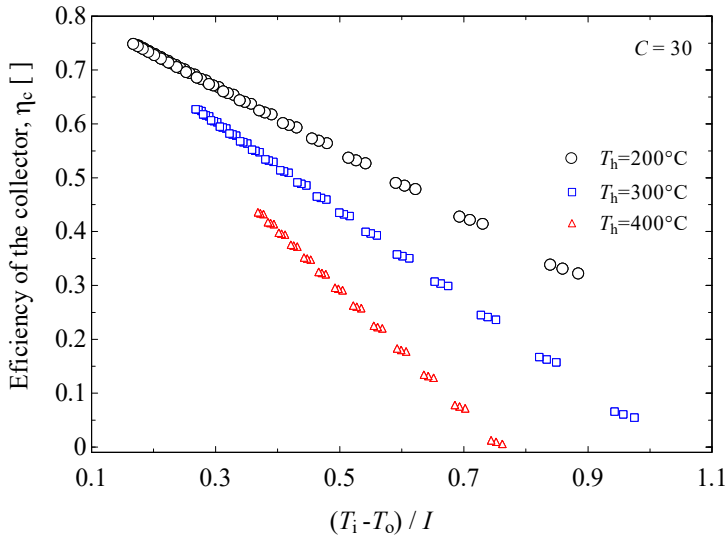

Figure 9. Efficiency of the solar concentrator with respect to $(T_i - T_o)/I$ at 3 hot spot temperatures.

To show the relationship between the performances of the different systems that compose the solar hybrid chiller, Figure 10 shows the efficiency of the solar concentrator, together with the COP of the two cooling systems, as a function of the solar radiation. In the figure, the solar concentrator efficiency is in the range from 0.33 to 0.75. COP of the absorption system is 0.85, while COP of the compression system is 11, when T_h = 200 °C, T_e = 10 °C and T_c = 28 °C.

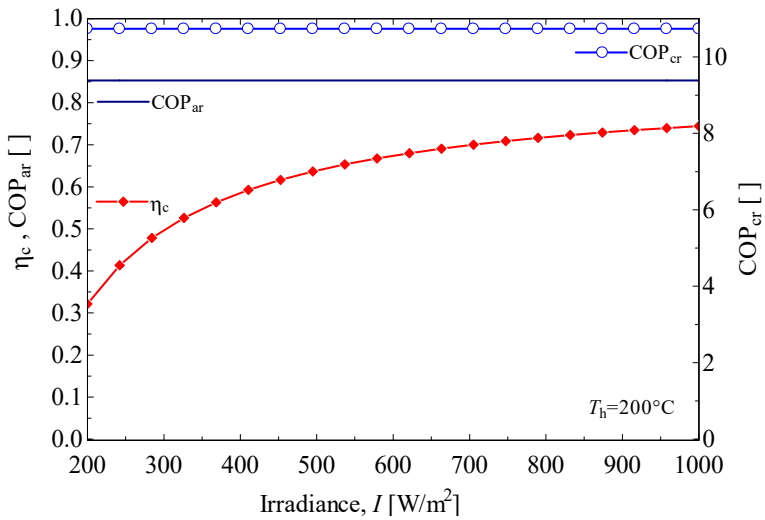

Figure 10. Efficiency of the solar collector and cooling systems, with respect to radiation in the solar concentrator.

The COP of the cooling systems and the collector efficiency are shown in Figure 11 as a function of T_h. In the figure, it can be seen that when T_e = 5 °C and T_c = 37 °C, the COP_{ar} increases from 0.27 to 0.78 approximately. However, when T_e = 10 °C and T_c = 28 °C, the change in COP_{ar} is negligible. The change in COP_{cr} is only appreciated with respect to T_c. Finally, the efficiency of the collector decreases as the collector temperature increases, as can be seen in the figure on the right side.

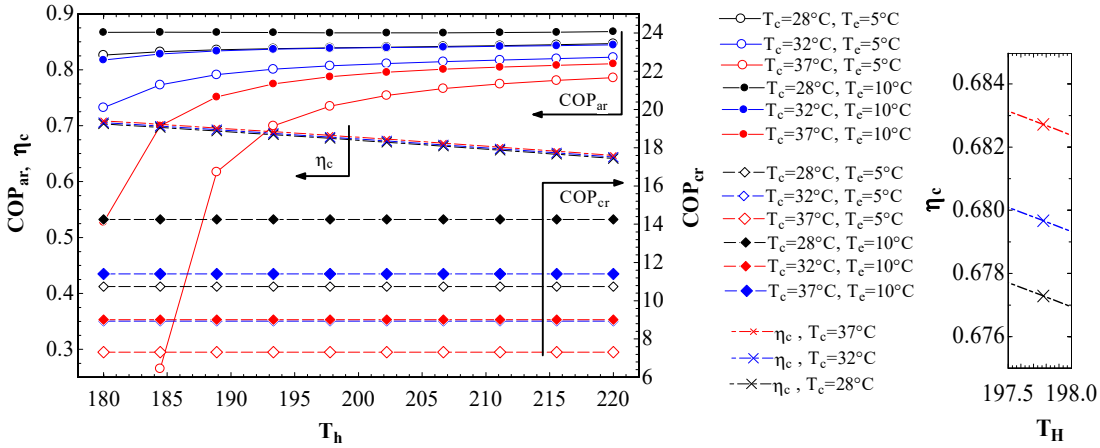

Figure 11. Efficiency of the solar collector and cooling systems, with respect to radiation in the solar concentrator.

The energy savings of the proposed hybrid chiller were determined in comparison to a commercial air conditioning equipment of 0.75 tons of refrigeration (2636 kW) [32]. The cooling capacity of the hybrid system is 2.72 kW (0.47 kW in the absorption evaporator and 2.25 kW in the compression evaporator). The electricity consumption of the compressor was 0.85 kW, taken from [32], while the electricity consumption of the solution pump was P_E = 0.032 kW, obtained from Figure 5, at the maximum recommended operating value of the absorption system, x_a = 0.4, with T_c = 37 °C and T_e = 15 °C ($P_E = P_p/\eta_p$ = 0.028/0.85). The cost of electricity in American dollars ($) per kWh in Mexico was taken from [33]. The energy savings of the proposed chiller, shown in Figure 12, were determined considering an operating period of 8 h per day, as recommended in [34], during 365 days per year. In Figure 12, it can be seen that electricity consumption of the conventional system is 26.6 times the consumption of the hybrid system. In cumulative values, with this difference in annual consumption, the energy savings with the proposed system is close to 60 MWh at the end of the equipment's useful life, 25 years.

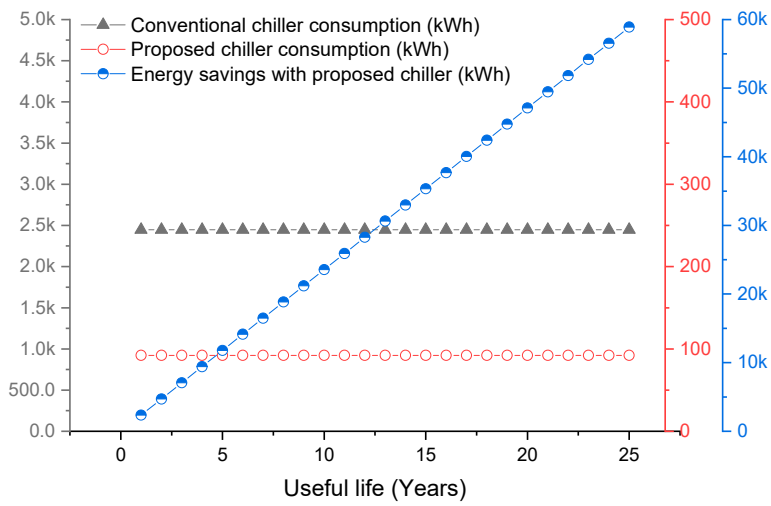

Figure 12. Energy savings caused by the proposed system.

The cost of operating the systems is shown in Figure 13. The initial cost of the proposed system was $3400 ($2000 absorption system, $800 Stirling engine and $600 solar collector). It can be seen from the figure that the operating cost of the conventional system is 26.6 times greater than that of the proposed system. Considering the cost of investment for the proposed system as negative and cumulative values, it can be seen that the recovery of the investment occurs in year 9. From that

moment, an economic saving of $5300 can be achieved at the end of the useful life of the proposed system, 25 years.

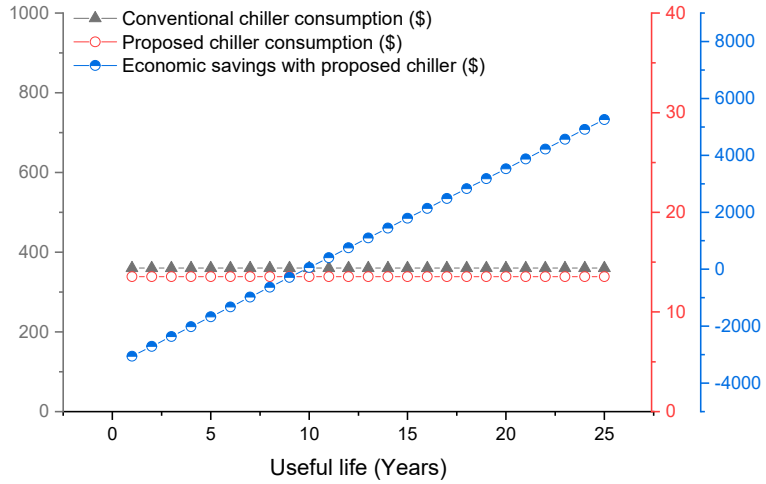

Figure 13. Economic savings caused by the proposed system.

4. Conclusions

From the modeling and simulation of the hybrid chiller and the solar concentrator, the following conclusions have been obtained:

Hybrid chiller for air conditioning.

- The hybrid chiller can produce cooling with both cooling systems coupled, or only with one, from $x_a = 0$ to $x_a = 1$.
- The compression system coupled with the Stirling engine can provide cooling power in the evaporator up to 53% higher than the heat supplied to the hot source of the heat engine.
- The mechanical power ratio between the compression and absorption system varies between 560 and 5 in the range of x_a from 0.05 to 0.95. When x_a is in the range of 0.2 to 0.45, the power ratio is between 130 and 30. This range may be suitable for the operation of the hybrid system.
- Regarding the heat ratio $r_q = \dot{Q}_u/\dot{Q}_e$, it can be concluded that for obtaining greater cooling power than heat supply, the operation of the absorption system should be between $x_a = 0.2$ and 0.6, with Stirling engine efficiencies between 0.2 and 0.3 and condensing temperatures from 28 to 37 °C.

Solar collector for hybrid chiller.

- The diameter of the absorber of the solar concentrator can be smaller than 30 cm, when the concentration ratio is greater than 20. This can contribute to distribute the radiation in the hot source over a larger area and to reach medium temperatures, rather than high temperatures, which contributes to improve the efficiency of the solar concentrator.
- The cooling power produced by the compression system can be up to 3 times higher than the heat supplied to the hot source of the Stirling engine, with $T_h = 200$ °C and $\eta_s = 0.3$.
- The efficiency of the solar concentrator is higher when the temperature in the hot spot is lower.
- With high T_c, the COP of the absorption system increases with T_h, whereas, with small T_c, the change in COP with respect to T_h is negligible.
- The energy and economic savings of the proposed system, respect to a conventional electricity-driven air conditioning system, can be up to 60 MWh and $5300 at the end of the useful life of 25 years.

Author Contributions: Conceptualization, G.R., C.J., J.d.J.R., A.Z. and M.V.; investigation, G.R., C.J., J.d.J.R., A.Z., I.C., J.A.J., J.P. and M.V.; resources, A.Z., I.C., J.A.J. and J.P.; writing—original draft preparation, G.R., C.J., J.d.J.R. and A.Z.; writing—review and editing, G.R., C.J., J.d.J.R., A.Z., I.C., J.A.J., J.P. and M.V.; funding acquisition, A.Z., I.C., J.A.J. and J.P. All authors have read and agreed to the published version of the manuscript.

Funding: This research was funded by National Polytechnic Institute of Mexico (IPN) Project (SIP20200538, 2082). G.R. and C.J. thanks CONACYT for the scholarship granted.

Conflicts of Interest: The authors declare no conflict of interest. The funders had no role in the design of the study; in the collection, analyses or interpretation of data; in the writing of the manuscript or in the decision to publish the results.

Nomenclature

A	area (m^2), absorber
ARS	Absorption Refrigeration System
C	concentration ratio, Condenser
SCS	Space conditioning system
COP	Coefficient of Performance
CRS	Compression refrigeration system
E	evaporator
G	generator
h	convection heat transfer coefficient (W/m^2K); enthalpy (kJ/kg)
I	solar irradiation (W/m^2)
$\dot{m}$	mass flow rate (kg/s)
$\dot{Q}$	heat flux (W)
R	recuperator
SES	Solar energy system
T	
TES	Thermal engine system
U	global heat transfer coefficient (W/m^2 K)
v	specific volume (m^3/kg)
x	concentration
w	specific work (kJ/kg)
$\dot{W}$	power (W)
Greek symbols	
η	performance
ε	efficiency, emissivity
σ	Boltzmann
Subscripts	
1, 2, 3 . . . 10	position in the system
a	absorber
Ab	solar absorber/heat spot
ae	absorption evaporator
App	parabolic dish
ar	absorption refrigeration
c	condenser/compression
cr	compression refrigeration
cs	concentrated solution
ds	diluted solution
D	driven
e	evaporator
ce	compression evaporator
inf	infiltration
g	generator
h	hot spot
HS	heat source of Stirling engine

i	indoor
LS	cold sink of Stirling engine
misc	miscellaneous
o	outside
oc	occupants
p	pump
r	radiation
re	recuperator
s	Stirling engine, surface
Sup	surface
t	transmission
T	total
u	useful

References

1. Krzaczek, M.; Florczuk, J.; Tejchman, J. Improved energy management technique in pipe-embedded wall heating/cooling system in residential buildings. *Appl. Energy* **2019**, *254*, 113711. [CrossRef]
2. Giacomin, R.; Calmon, J.L.; Viera, D.; Chain, M.C. Characterization of representative residential buildings within a neighborhood and their energy efficiency levels according to RTQ-R. *Appl. Sci.* **2019**, *9*, 3832. [CrossRef]
3. Brennenstuhl, M.; Zeh, R.; Otto, R.; Pesch, R.; Stockinger, V.; Pietruschka, D. Report on a plus-energy district with low-temperature dhc network, novel agrothermal heat source, and applied demand response. *Appl. Sci.* **2019**, *9*, 5059. [CrossRef]
4. Pater, S. Field measurements and energy performance analysis of renewable energy source devices in a heating and cooling system in a residential building in southern Poland. *Energy Build.* **2019**, *199*, 115–125. [CrossRef]
5. Sen, O.; Yilmaz, C. Thermodynamic performance analysis of geothermal and solar energy assisted power generation and residential cooling system. *Int. Adv. Res. Eng. J.* **2020**, *4*, 41–47. [CrossRef]
6. Inayat, A.; Raza, M. District cooling system via renewable energy sources: A review. *Renew. Sustain. Energy Rev.* **2019**, *107*, 360–373. [CrossRef]
7. Bergero, S.; Chiari, A. On the performances of a hybrid air-conditioning system in different climatic conditions. *Energy* **2011**, *36*, 5261–5273. [CrossRef]
8. Ni, M.; Shi, B.; Xiao, G.; Peng, H.; Sultan, U.; Wang, S.; Luo, Z.; Cen, K. Improved Simple Analytical Model and experimental study of a 100 W β-type Stirling engine. *Appl. Energy* **2016**, *169*, 768–787. [CrossRef]
9. Tongdee, N.; Jandakaew, M.; Dolwichai, T.; Thumthae, C. Thermodynamics Analysis for Optimal Geometrical Parameters and Influence of Heat Sink Temperature of Gamma-configuration Stirling Engine. *Energy Procedia* **2017**, *105*, 1782–1788. [CrossRef]
10. Cascella, F.; Sorin, M.; Formosa, F.; Teyssedou, A. Modeling the dynamic and thermodynamic operation of Stirling engines by means of an equivalent electrical circuit. *Energy Convers. Manag.* **2017**, *150*, 295–303. [CrossRef]
11. Wang, J.; Wang, B.; Wu, W.; Li, X.; Shi, W. Performance analysis of an absorption-compression hybrid refrigeration system recovering condensation heat for generation. *Appl. Therm. Eng.* **2016**, *108*, 54–65. [CrossRef]
12. Yang, H.S.; Cheng, C.H. Stability analysis of thermal-lag Stirling engines. *Appl. Therm. Eng.* **2016**, *106*, 712–720. [CrossRef]
13. Chahartaghi, M.; Sheykhi, M. Thermal modeling of a trigeneration system based on beta-type Stirling engine for reductions of fuel consumption and pollutant emission. *J. Clean. Prod.* **2018**, *205*, 145–162. [CrossRef]
14. Açıkkalp, E.; Kandemir, S.Y.; Ahmadi, M.H. Solar driven Stirling engine—chemical heat pump—absorption refrigerator hybrid system as environmental friendly energy system. *J. Environ. Manag.* **2019**, *232*, 455–461. [CrossRef] [PubMed]
15. Li, J.; Xu, S. The performance of absorptionecompression hybrid refrigeration driven by waste heat and power from coach engine. *Appl. Therm. Eng.* **2013**, *61*, 747–755. [CrossRef]

16. Li, Z.; Yu, J.; Chen, E.; Jing, Y. Off-design modeling and simulation of solar absorption-subcooled compression hybrid cooling system. *Appl. Sci.* **2018**, *8*, 2612. [CrossRef]
17. Fitó, J.; Coronas, A.; Mauran, S.; Mazet, N.; Stitou, D. Definition and performance simulations of a novel solar-driven hybrid absorption-thermochemical refrigeration system. *Energy Convers. Manag.* **2018**, *175*, 298–312. [CrossRef]
18. Mohammadi, K.; Efati Khaledi, M.S.; Powell, K. A novel hybrid dual-temperature absorption refrigeration system: Thermodynamic, economic, and environmental analysis. *J. Clean. Prod.* **2019**, *233*, 1075–1087. [CrossRef]
19. Song, M.; Wang, L.; Yuan, J.; Wang, Z.; Li, X.; Liang, K. Proposal and parametric study of solar absorption/dual compression hybrid refrigeration system for temperature and humidity independent control application. *Energy Convers. Manag.* **2020**, *220*, 113107. [CrossRef]
20. He, H.; Wang, L.; Yuan, J.; Wang, Z.; Fu, W.; Liang, K. Performance evaluation of solar absorption-compression cascade refrigeration system with an integrated air-cooled compression cycle. *Energy Convers. Manag.* **2019**, *201*, 112153. [CrossRef]
21. Zhang, J.; Li, Z.; Chen, H.; Xu, Y. Effect of hotwater setting temperature on performance of solar absorption-subcooled compression hybrid cooling systems. *Appl. Sci.* **2020**, *10*, 258. [CrossRef]
22. Zhang, J.; Li, Z.; Jing, Y.; Xu, Y. Performance of solar absorption-subcooled compression hybrid cooling system for different flow rates of hot water. *Appl. Sci.* **2020**, *10*, 810. [CrossRef]
23. Lin, L.; Tian, Y.; Luo, Y.; Chen, C.; Jiang, L. A novel solar system integrating concentrating photovoltaic thermal collectors and variable effect absorption chiller for flexible co-generation of electricity and cooling. *Energy Convers. Manag.* **2020**, *206*, 112506. [CrossRef]
24. Lee, Y.; Park, S.; Kang, S. Performance analysis of a solid desiccant cooling system for a residential air conditioning system. *Appl. Therm. Eng.* **2021**, *182*, 116091. [CrossRef]
25. Arzoz, D.; Rodriguez, P.; Izquierdo, M. Experimental study on the adiabatic absorption of water vapor into LiBr-H_2O solutions. *Appl. Therm. Eng.* **2005**, *25*, 797–811. [CrossRef]
26. Herold, K.E.; Radermacher, R.; Klein, S.A. *Absorption Chillers and Heat Pumps*, 2nd ed.; CRC Press: Columbus, OH, USA, 2016; ISBN 978-1498714341.
27. Zacarías, A.; Quiroz, J.A.; Gutiérrez-Urueta, G.L.; Venegas, M.; Carvajal, I.; Rubio, J. Comparison between adiabatic and non-adiabatic absorption chillers using ammonia-lithium nitrate and water-lithium bromide solutions. *Heat Transf. Res.* **2020**, *51*, 609–621. [CrossRef]
28. Dai, D.; Liu, Z.; Yuan, F.; Long, R.; Liu, W. Finite time thermodynamic analysis of a solar duplex Stirling refrigerator. *Appl. Therm. Eng.* **2019**, *156*, 597–605. [CrossRef]
29. Barreto, G.; Canhoto, P. Modelling of a Stirling engine with parabolic dish for thermal to electric conversion of solar energy. *Energy Convers. Manag.* **2017**, *132*, 119–135. [CrossRef]
30. Klein, S.A. *Engineering Equation Solver*; F-Chart Software: Madison, WI, USA, 2018.
31. Reyes, J.; Zacarías, A.; Jiménez, J.A.; Donís, F.; Gutiérrez, C. *Modelado de un Colector Solar Parabólico con Motor Stirling Para uso Doméstico y Pequeña Industria*; XXIV Congreso Internacional Anual de la SOMIM; SOMIM: Campeche, Mexico, 2018; pp. 145–150.
32. Click Renovables. Available online: https://clickrenovables.com/blog/aire-acondicionado-eficiente/ (accessed on 4 December 2020).
33. Globalpetrolprice. Available online: https://es.globalpetrolprices.com/electricity_prices/ (accessed on 4 December 2020).
34. Goswami, D.Y. *Principles of Solar Engineering*, 3rd ed.; CRC Press: New York, NY, USA, 2015; ISBN 9781466563797.

Publisher's Note: MDPI stays neutral with regard to jurisdictional claims in published maps and institutional affiliations.

© 2020 by the authors. Licensee MDPI, Basel, Switzerland. This article is an open access article distributed under the terms and conditions of the Creative Commons Attribution (CC BY) license (http://creativecommons.org/licenses/by/4.0/).